Numerical and Experimental Analysis of the Anisotropy Evolution in Aluminium Alloys Processed by Asymmetric Rolling

Gabriela Vincze[1,2,*], Augusto Lopes[3], Marilena C. Butuc[1,2],
Jesús Yánez[1], Diogo Lopes[1], Laura Holz[1], Ana Graça[1]
and António B. Pereira[1,2]

[1]*Centre of Mechanical Technology and Automation (TEMA), Department of Mechanical Engineering, University of Aveiro, 3810-193 Aveiro, Portugal*
[2]*LASI – Intelligent Systems Associate Laboratory, Portugal*
[3]*Department of Materials and Ceramic Engineering, CICECO, University of Aveiro, 3810-193 Aveiro, Portugal*
E-mail: gvincze@ua.pt
[*]*Corresponding Author*

Abstract

One of the most important characteristics of the sheet metal is its anisotropy. Asymmetric rolling (ASR) shows to be an adequate process to change the material anisotropy by increasing the normal anisotropy and decreasing the planar anisotropy. In this work, it is analysed the relationship between anisotropy and texture evolution using experimental and numerical approaches. Experimentally, the texture is modified by rolling, involving symmetric (SR), asymmetric rolling continuous (ARC) and asymmetric reverse (ARR) routes and different reductions per pass. The numerical analysis was performed through the visco-plastic self-consistent model where two hardening laws were considered, namely the Voce-type (V) and the dislocation density-based model (DDR). The main objective of the numerical

method was to test the performance of the VPSC model for large plastic deformation. The Lankford coefficients decrease in RD and increase in TD with the increase in the total thickness reduction. This trend observed experimentally is well captured by the VPSC model, however, in terms of R-value, an overestimation is observed in both cases with better results for Voce-type law.

Keywords: Anisotropy, texture, aluminium alloys, rolling, visco-plastic self-consistent model.

1 Introduction

Aluminium alloys play a key role in the actual environmental conditions. Its light-weighting and strength, as well as the high capability for recyclability over and over without degradation, make aluminium alloy a top material for several applications from aerospace and automotive industries to packaging. Many of these applications involve plastic deformations. In sheet metal forming, plastic anisotropy is one of the most important parameters. Linked to two main sources, i.e. microstructural characteristics of grains and grain boundaries, and crystallographic texture, the latter is much more significant, being a topic extensively investigated over the years. On one hand, investigation has been focuses on the developing methods to produce sheet metal with desired anisotropy. Thus, new technics such as Equal channel angular extrusion (ECAP) for billets or asymmetric rolling for plates and sheets arose. On the other hand, a large effort has been made to develop models which accurately describe the mechanical behaviour of materials and consequently their anisotropy. The anisotropy can be described by analytical yield criteria such the ones developed by Hill [1], Barlat et al. [2, 3], Banabic [4], Cazacu, and Barlat [5–7] or by crystal plasticity models based on the crystallographic orientations of the grains such the ones developed by Sachs [8], Taylor [9], Tome and Lebenson [10] visco-plastic self-consistent model and Van Houtte [11] ALAMEL model. Recently, Cazacu et al. [12] developed an analytical single crystal criterion capable to predict the material anisotropy of polycrystals.

Regarding the experimental work, the improvement of anisotropy through ASR is stated by several authors. ASR is a type of rolling in which the upper surface of the sheet is forced to pass faster between the rolls of the mill compared to the lower surface of the sheet. In this way, an asymmetry is created along the sheet thickness. The three methods that are usually

applied to create this asymmetry are the differences in the diameters of the rolls, angular speed, or friction coefficients [13]. Sidor et al. [14] found that a ratio of 1.5 between the roll's diameters, leads to a formation of shear texture components in AA6016 which improves the planar and normal anisotropy values. Wronsky and co-workers [15] succeeded increased the anisotropy of AA6061 by ASR but the gain was diminished during recrystallization. They used the finite element commercial software ABAQUS coupled to the Leffers-Wierzbanowski (LW) model to predict deformation texture [16]. An increase of the normal anisotropy $\overline{R}$-value (defined by $\overline{R} = (R_0 + R_{90} + 2R_{45})/4$) about 1.3 times and decrease the planar anisotropy DR (define by $\Delta R = (R_0 + R_{90} - 2R_{45})/2$) to 0.02 from 0.66 was achieved by Lee and co-works [17] in AA1050. The improvement anisotropy was associated to the reduction of the rotate cube $\{001\}\langle110\rangle$ and increase of the $ND//\langle111\rangle$ texture components. Tamimi et al. [18] obtained an increase in the R-value of AA5182 after rolling but the planar anisotropy was also increased, which means that the earing profile would be more pronounced in this sheet. They used the VPSC model to predict the mechanical behaviour after rolling. The VPSC model was also used by Dhinwal and Toth [19] to study asymmetric rolled low carbon steel sheets and they observed that simulating rolling and shear in different steps resulted in better texture predictions than simulating both deformation processes simultaneously. The analyses of plastic anisotropy and texture evolution during rolling process was carefully investigated by Shore et al. [20], using the FACET/ALAMEL approach. Their results suggest that the ASR in the last steps is more favourable for a preferred texture than ASR from the early steps of the rolling.

In the present work, we study the evolution of anisotropy with rolling conditions by experimental and numerical means. The rolling conditions involve symmetry and non-symmetry of the process, variation of the reduction per pass and change of strain path through the rolling routes. The relationship within Lankford coefficient and texture evolution is analysed. For the numerical part, it was used the VPSC code.

2 Material and Methodology

2.1 Material and Experimental Details

The material selected in this study is a heat treatable Al-Mg-Si alloys 6022, natural aged produced by Alcoa for the automotive industry. The main chemical components added to aluminium are Si (0.8–1.5%), Fe (0.05–0.2%),
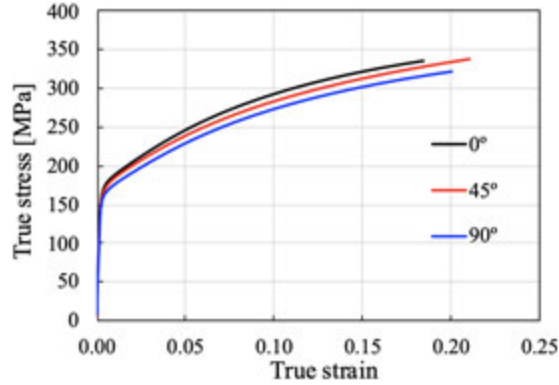
Figure 1   Stress-strain curve of the as-received material.
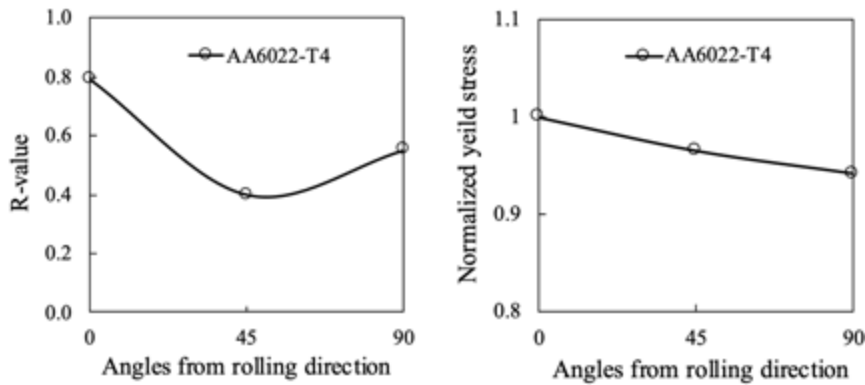
Figure 2   R-value (left) and normalized yield stress (right) of the as received material.

Cu (0.01–0.11%), Mn (0.02–0.1%), Mg (0.45–0.7%), Cr (0.1%), Zn (0.25%), Ti (0.15%) and other 0.15%. The as received material has a 2 mm thickness and it is characterized by a yield stress about 162–172 MPa and ultimate tensile stress about 263–277 MPa. The uniform deformation and total deformation are about 20–24% and 30–33% respectively. The material is anisotropic as it can be seen in Figure 1, where the stress-strain curves of material tested in uniaxial tension at 0°, 45° and 90° from the rolling direction are represented.

The Lankford coefficient (ratio of the width and thickness strains) reach a maximum for rolling direction (RD or 0°) and the minimum for diagonal direction (DD or 45°) with transverse direction (TD or 90°) between, as can be seen in Figure 2(a). The material shows a very weak anisotropy in yield
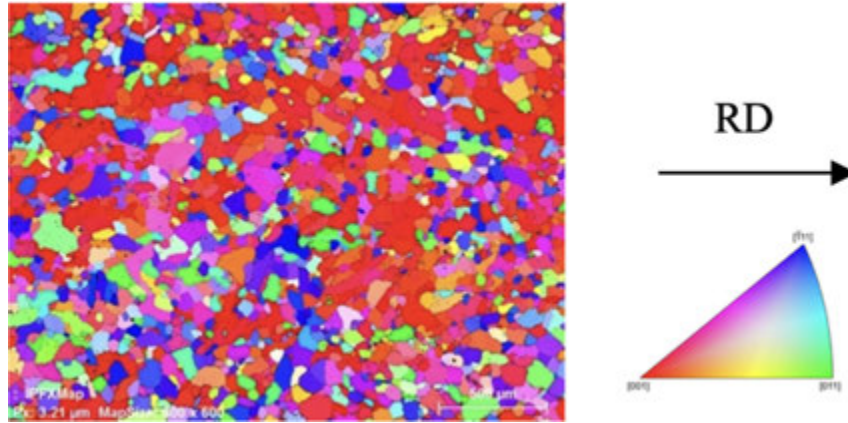
Figure 3   EBSD orientation map of the initial material.

stress, with a small linear decrease from RD to TD direction as it can be confirmed in Figure 2(b). The material was tested in uniaxial tensile test with strain rate $10^{-3}s^{-1}$ using a Shimadzu AG-100kN (Japan). The strain was measured by Digital Image Correlation using the GOM system and Aramis 5M software (Germany).

The grains orientations of the initial material, represented in Figure 3, were mapping by the Electron Backscatter Diffration (EBSD) using a Bruker CrystAlign QC 400 EBSD system connected to a Hitachi SU-70 SEM (Japan). From the EBSD raw data, a set of 1000 crystallographic orientation grains were extracted with Matlab-MTEX free toolbox [21] and generated the pole figures and the ODF sections represented in the Euler angles φ_1, Φ and φ_2. The results are presented in Figure 4 and show a strong {100} <001> preferential crystallographic orientation of the grains, typical of recrystallized aluminium sheets. The presence of this texture component, known as a cube component, is associated to a low $\overline{R}$ and a high ΔR values that impairs the aluminium sheet drawability.

2.2 Asymmetric Rolling

Asymmetric rolling was produced by the difference in the speeds between the upper roll and bottom roll of the mill. In this work, it was used a ratio of 1 corresponds to symmetric rolling (SR) and a ratio of 1.36 corresponds to asymmetric rolling (AR) obtained by the angular speed 15 rpm/15 rpm and 15 rpm/11 rpm. Besides it, the total thickness reduction for all the cases was 50%, obtained in 2 or 4 passes, with a thickness reduction per pass of
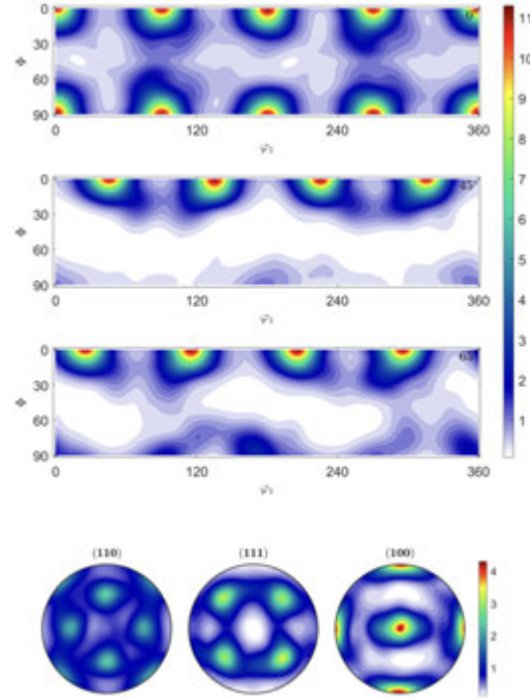
Figure 4   ODF sections for φ_2 iqual to $0°$ (top), $45°$ (middle), and $65°$ (bottom) and the pole figures {110},{111},{100} of the initial material.

30% and 15%, respectively. Regarding the asymmetric rolling, two types of strain paths were studied, produced by the rotation of the sheet between two subsequent passes. Namely, without rotation, it was generated the route called asymmetric continuous (ARC) and with rotation of $180°$ around the RD it was generated the asymmetric reverse route (ARR). The effect of the rolling route affects principally the shear deformation formed in sheet thickness, being forward or reverse for ARC and ARR respectively. A schematic of the asymmetric process is represented in Figure 5, and the experimental rolling parameters are presented in Table 1.

2.3 Modelling

The viscoplastic self-consistent model developed by Lebenson and Tome [22–24] which compute the macroscopic response of the polycrystals from the contribution of each grain is used in this work. The diagram of the modelling is presented in Figure 6.
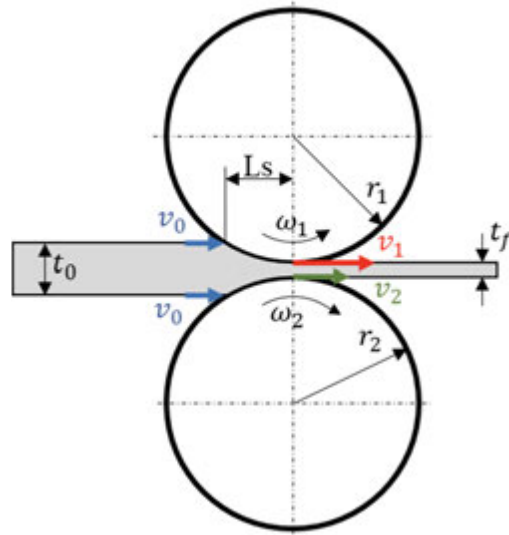
Figure 5   Asymmetric rolling schematic.

Table 1   Experimental rolling parameters

Constants	Values
r_1 (top roll radius)	90 mm
r_2 (bottom roll radius)	90 mm
ω_1 (top roll angular velocity)	15 rpm
ω_2 (bottom roll angular velocity)	11 rpm
t_0 (initial thickness)	2 mm

Brief Description of VPSC

In the self-consistent crystal plasticity model, each grain is considered as an inhomogeneous inclusion embedded in the "homogeneous effective medium" (HEM) which has the characteristics of the polycrystal. Thus, the macroscopic response of the polycrystals results from the contribution of each grain. At the single crystal level, the strain rate is calculated according to the slip activations

$$d^g = \sum_s m^s \dot{\gamma}^s = \dot{\gamma}_0 \sum_s m^s \left(\frac{m^s \sigma^g}{\tau^s} \right)^n \tag{1}$$

where, m^s is the symmetric part of Schmid tensor, $\dot{\gamma}^s$ is the shear rate, $\dot{\gamma}_0$ is a normalized shear rate, n is the inverse strain-rate sensitivity, τ^s is the critical resolved shear stress CRSS. The relationships between strain-rate and stress
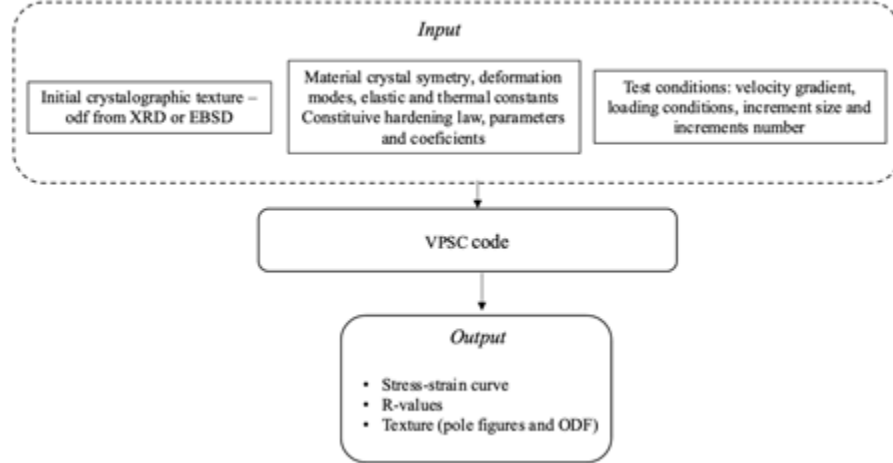
Figure 6　Diagram of the modelling.

for single crystal and for the polycrystal are written in a linearised form as:

$$d^g = M^g \sigma^g + d_0^g$$

$$D = \bar{M}\Sigma + D_0 \tag{2}$$

where M^g and $\bar{M}$ are the local and macroscopic compliance tensors, d_0^g and D_0 are the back-extrapolated terms for the grain and for the polycrystal, respectively. The inclusion formalism provides the interaction between a grain and the polycrystal in terms of local and average stress and strain rate, as:

$$(d^g - D) = -\tilde{M}(\sigma^g - \Sigma) \tag{3}$$

where

$$\tilde{M} = n^{eff}(I - E)^{-1} : E : \bar{M}^{secant} \tag{4}$$

d^g and σ^g are the deviatoric strain-rate and stress at the single crystal level and D and Σ are the macroscopic strain-rate and stress, respectively. E represents the Eshelby tensor for a particular grain. $\bar{M}^{secant}$ is the macroscopic visco-plastic compliance tensor for the secant case. The parameter n^{eff} describes the visco-plastic compliance of the inclusion-matrix interactions $n^{eff} = 0$ for a Taylor case, $n^{eff} = 1$ for a Secant case and $n^{eff} = n$ for a Tangent case [22, 23]. In this work it was considered the Tangent interaction with $n = 10$.

Material Modelling

In this work, two hardening laws were considered, namely an extended Voce-type law and the dislocation based hardening model. The parameters were determined by fitting of the stress-strain curve of the initial material tested in RD. The Voce-type law is presented in Equation (5):

$$\tau = \tau_0 + (\tau_1 + \theta_1 \Gamma) \left[1 - exp \left(-\Gamma \left| \frac{\theta_0}{\tau_1} \right| \right) \right], \tag{5}$$

where τ is the threshold resolved shear stress, and its evolution depends on the accumulated shear strain, Γ, in each grain, τ_0 is the initial critical resolved shear stress (CRSS), θ_0 is the initial hardening rate, θ_1 is the asymptotic hardening rate, and $(\tau_0 + \tau_1)$ is the back-extrapolated CRSS [24, 25]. The values used in the simulations are presented in Table 2.

Table 2   Material coefficients of the Voce-type model for the AA6022-T4 alloy

τ_0	τ_1	θ_0	θ_1
56.4	87.5	333.0	0.42

The dislocation-based hardening model is a model which account for the strain path changes and considers dislocations accumulation and annihilation, and back-stress phenomena. The model proposed initially for a continuum by Rauch et al. [26], was transformed by Kitayama et al. [27] in a crystallographic model where the track of dislocation in each system of each grain is accounted. Later the back-stress effect was added by Wen and co-workers [27]. In this work, this later version of the model is used, in which the CRSS on the slip system s (τ^s) is expressed as:

$$\tau^s = \tau_d^s + \Delta \tau_B^s \tag{6}$$

where $\Delta \tau_B^s$ is associated to the contribution of back-stress and τ_d^s is calculated through the Taylor law.

$$\tau_d^s = \tau_0^s + \mu b \sqrt{\alpha^{ss} \rho^s + \sum_{s \neq s'} \alpha^{ss'} \rho^{s'}} \tag{7}$$

where τ_0^s is the initial CRSS, μ, b and ρ^s denote the shear modulus, the magnitude of the Burgers vector and the total dislocation density for slip system s, respectively. $\alpha^{ss'}$ is the latent hardening matrix.

The dislocation density on the slip system s is decomposed in three components as follows:

$$\rho^s = \rho_{for}^s + \rho_{rev}^{s+} + \rho_{rev}^{s-} \tag{8}$$

where ρ^s is total dislocation density on slip system s, ρ^s_{for} is the forward dislocation density, ρ^{s+}_{rev} and ρ^{s-}_{rev} are the reversible dislocation density on s^+ and s^-, respectively. The total dislocation density in one grain is given by the sum of the dislocation density in each grain.

$$\rho = \sum_s \rho^s = \sum_s (\rho^s_{for} + \rho^{s+}_{rev} + \rho^{s-}_{rev}) \tag{9}$$

The back-stress effect on each slip system is introduced as a linear correction of the τ^s_d through the relations:

$$\Delta\tau^s_B = -\tau^s_d f^s_B \left(\frac{\rho^{s-}_{rev}}{\rho_{total}} \right) \quad \text{if } d\gamma^+ > 0$$

$$\Delta\tau^s_B = -\tau^s_d f^s_B \left(\frac{\rho^{s+}_{rev}}{\rho_{total}} \right) \quad \text{if } d\gamma^- > 0 \tag{10}$$

Which led to a new formulation of Equation (6):

$$\tau^s = \tau^s_d + \Delta\tau^s_B = \tau^s_d \left[1 - f^s_B \left(\frac{\rho^{s- \, (+)}_{rev}}{\rho_{total}} \right) \right] \quad \text{if } d\gamma^{+(-)} > 0 \tag{11}$$

The constants of DDR model used in this work are presented in Table 3.

Figure 7 shows the fitting curves compared to experimental data where it can be seen that both numerical models are able to describe the hardening behaviour of the AA6022-T4 alloy.

Table 3   Material constants of the DDR model for the AA6022-T4 alloy

Constants	Values
μ (Elastic shear modulus)	24.0 GPa
b (Burgers vector)	2.86e-10
D (Grain size)	10 μm
τ_0 (Initial CRSS)	55 MPa
K (Mobile to storage parameter)	83
f (Recombination parameter)	3.4
ρ_{min} (Lower reversibility threshold)	1.0e12
ρ_{max} (Lower reversibility threshold)	7.0e14
f^S_B (Back-stress parameter)	0.5
q (Back-stress parameter)	2
m (Recombination rate parameter)	0.3
$\alpha^{SS'}$ (Latent hardening matrix)	1.0 (S = S') 0.45 (S $\neq$ S')
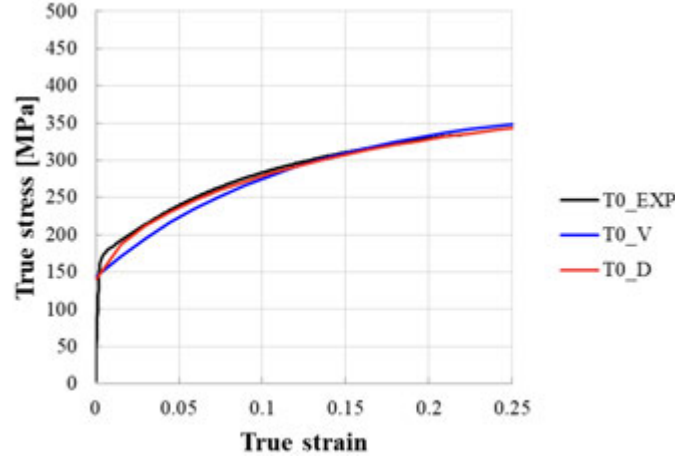
Figure 7   Fitting stress-strain curves for the DDR (D) and Voce-type (V) strain hardening rules.

Boundary Conditions

The boundary conditions prescribe the strain and stress components. For a symmetric rolling test, a plain-strain condition is considered, and the corresponding reduction strain is incrementally imposed in the normal direction. Assuming that $|\varepsilon|$ is the absolute value of the strain in the normal direction, caused by the thickness reduction, and L is the macroscopic velocity gradient, the strain tensor can be written as follows:

$$\varepsilon_{ij} = \begin{bmatrix} \varepsilon_{11} & \varepsilon_{12} & \varepsilon_{13} \\ \varepsilon_{21} & \varepsilon_{22} & \varepsilon_{23} \\ \varepsilon_{31} & \varepsilon_{32} & \varepsilon_{33} \end{bmatrix} = \frac{1}{2} \begin{bmatrix} 2\varepsilon_{11} & \gamma_{12} & \gamma_{13} \\ \gamma_{21} & 2\varepsilon_{22} & \gamma_{23} \\ \gamma_{31} & \varepsilon_{\gamma 32} & 2\varepsilon_{33} \end{bmatrix} = |\varepsilon|\, L, \qquad (12)$$

Where indices 1, 2, and 3 correspond to the rolling direction (RD), transverse direction (TD), and normal direction (ND), respectively. The normalized velocity gradient for rolling conditions can be stated as:

$$L = \begin{bmatrix} 1 & 0 & p \\ 0 & 0 & 0 \\ 0 & 0 & -1 \end{bmatrix}, \qquad (13)$$

where p represents the presence of shear:

– p = 0 the process is symmetric,
– p ≠ 0 the process is asymmetric,

and $|\varepsilon|$ is a function of the thickness reduction percentage, %Red, as follows:

$$|\varepsilon| = abs\left[ln\left(1 - \frac{\% \, Red}{100}\right)\right]. \quad (14)$$

Shear strain can be determined empirically or analytically. In experiments, the shear angle can be measured by the angle formed by the initial position – Figure 8(a) and the final position – Figure 8(b) of a line drawing on the sheet thickness perpendicular to the top and bottom surfaces. After the asymmetric rolling process, this line will present a slope, as represented in Figure 8(c). The relation between the slope angle and the shear deformation is shown in Equation (15).

$$p = \pm\frac{\gamma_{13}}{\varepsilon_{33}}, \quad \text{where } \gamma_{13} = tan(\theta). \quad (15)$$
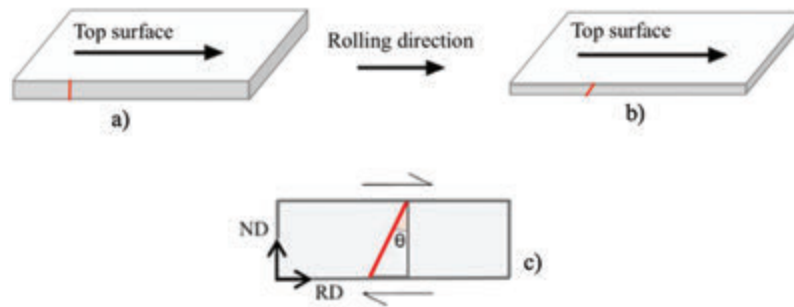
Figure 8   Shear deformation scheme (q is the shear angle).

Analytically, shear strain can be determined as [28]:

$$\gamma_{13} = 4L_s C_\omega \frac{t_0 - t_f}{(t_0 + t_f)^2}, \quad \text{with} \quad (16)$$

$$C_\omega = \frac{\omega_1 r_1 - \omega_2 r_2}{\omega_1 r_1 + \omega_2 r_2}, \quad \text{and} \quad (17)$$

$$L_s = \sqrt{R(t_0 - t_f) - \left(\frac{t_0 - t_f}{2}\right)^2}, \quad (18)$$

where t_0 and t_f are the initial and final thickness, ω and r are the angular velocities and radii of rolls, where indices 1 and 2 are related to the top and bottom rolls, respectively, and R is an equivalent radius that can be

determined as:

$$R = \frac{2r_1 r_2}{r_1 + r_2}. \tag{19}$$

As mentioned before, the thickness reductions of 15% and 30% were considered, in multi-step processes of four (4) and two (2) steps, respectively. The shear strain values used in simulations were determined analytically. The parameters are summarized in Table 4.

Table 4   Rolling tests parameters for the VPSC model

Simulations Processes Parameters		Thickness Reduction (ND)	
		15%	30%
$|\varepsilon|$	Equation (14)	≈0.16	≈0.36
γ_{13}	Equation (16)	± 0.07	± 0.23
θ [°]	Equation (15)	± 4.0	± 13.2
p	Equation (15)	± 0.43	± 0.66

It must be noted, in the first step of the asymmetric rolling process, p > 0. For the continuous asymmetric rolling simulations, p > 0 in all subsequent steps. For the asymmetric rolling-reverse, p < 0 for even steps and p > 0 for odd steps.

3 Results and Discussion

R-values after rolling are presented in Figure 9. A reduction of R_0 occurs for all the rolling routes while R_{90} increases. This transition of R-values on the sheet plane occurs in a direction between 15° and 30° from the RD and it is observed for experimental data as well as for numerical results, for both hardening laws as can be seen in Figures 10 and 11, corresponding to Voce and DDR, respectively. The numerical results, reproduce the experimental trend, but the values are higher than the measured ones. Moreover, while the results obtained with Voce hardening law keep the relative position regarding the evolution of the R-value corresponding to the initial material, the results obtained with DDR overestimated all the R-values, placing all the curves above the curve corresponding to the initial material. Thus, although DDR law was expected to return more accurate values, this is not verified, and it seems that in this case the Voce hardening type is recommended.

The normal anisotropy and the planar anistropy are represented in Figures 15 and 16 for 15% thickness reduction per pass and 30% reduction per pass, respectively. It can be seen that the experimental $\overline{R}$ and ΔR
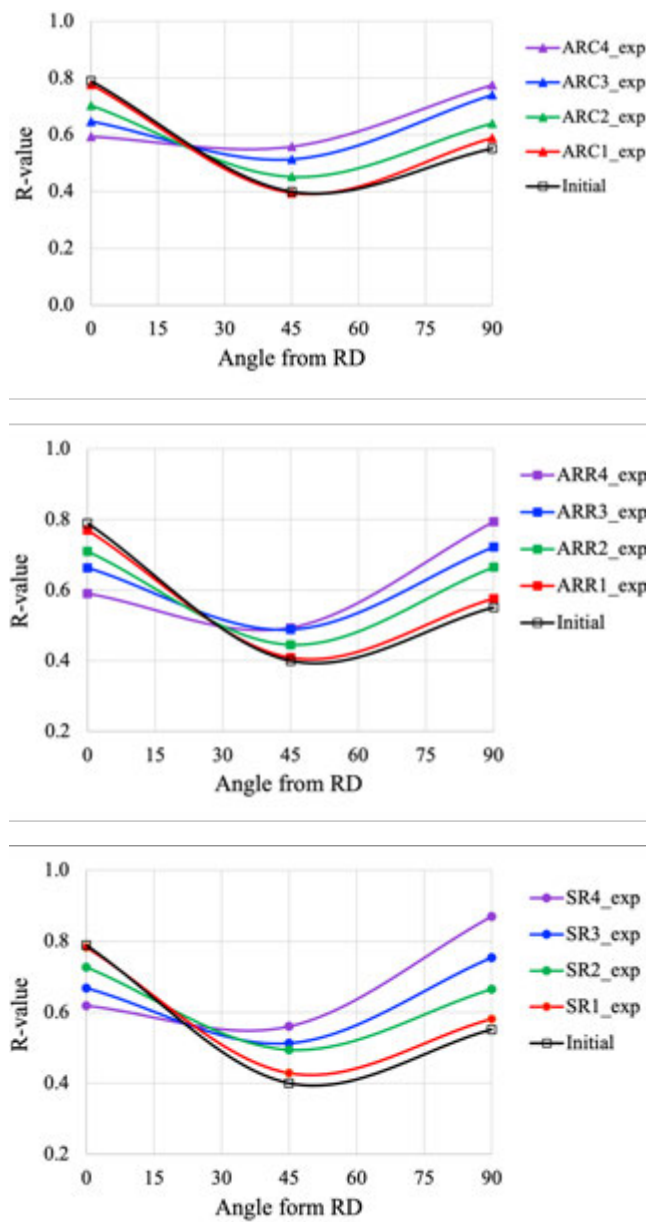
Figure 9   Evolution of Lanckford coefficient with rolling. Experimental data for 15% thickness reduction per pass of ARC (top), ARR (middle), and SR (bottom).
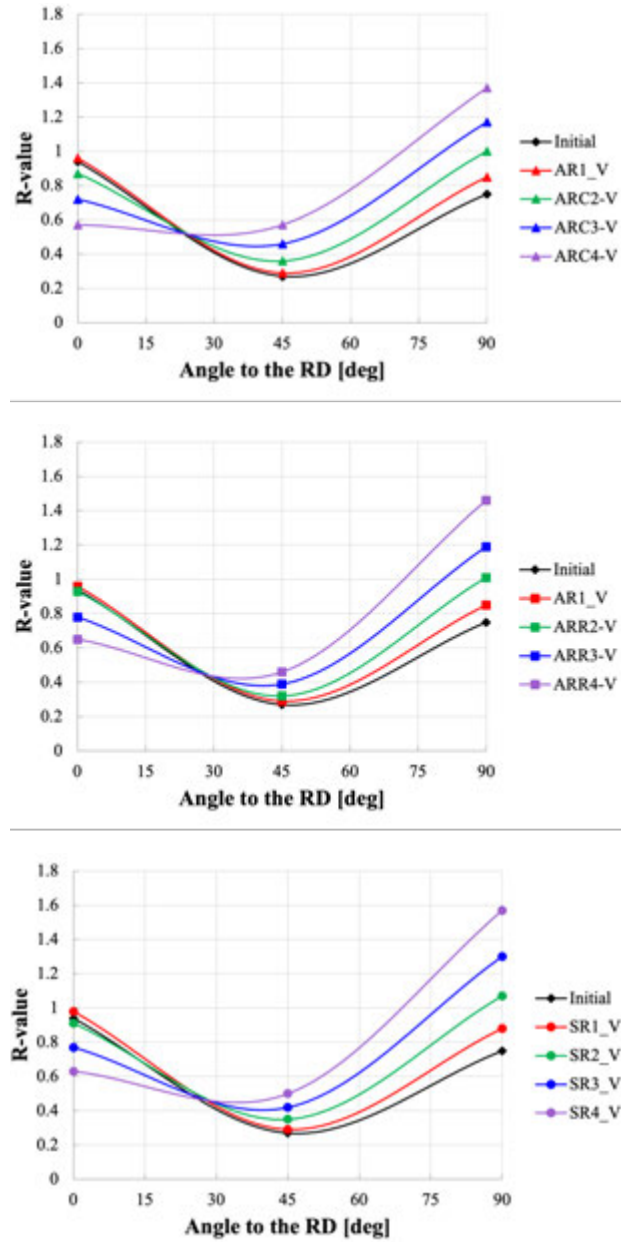
Figure 10 Simulated R-values of four-pass sequences rolling with a 15% thickness reduction per pass of ARC (top), ARR (middle), and SR (bottom) processes using a Voce-type hardening law (V).
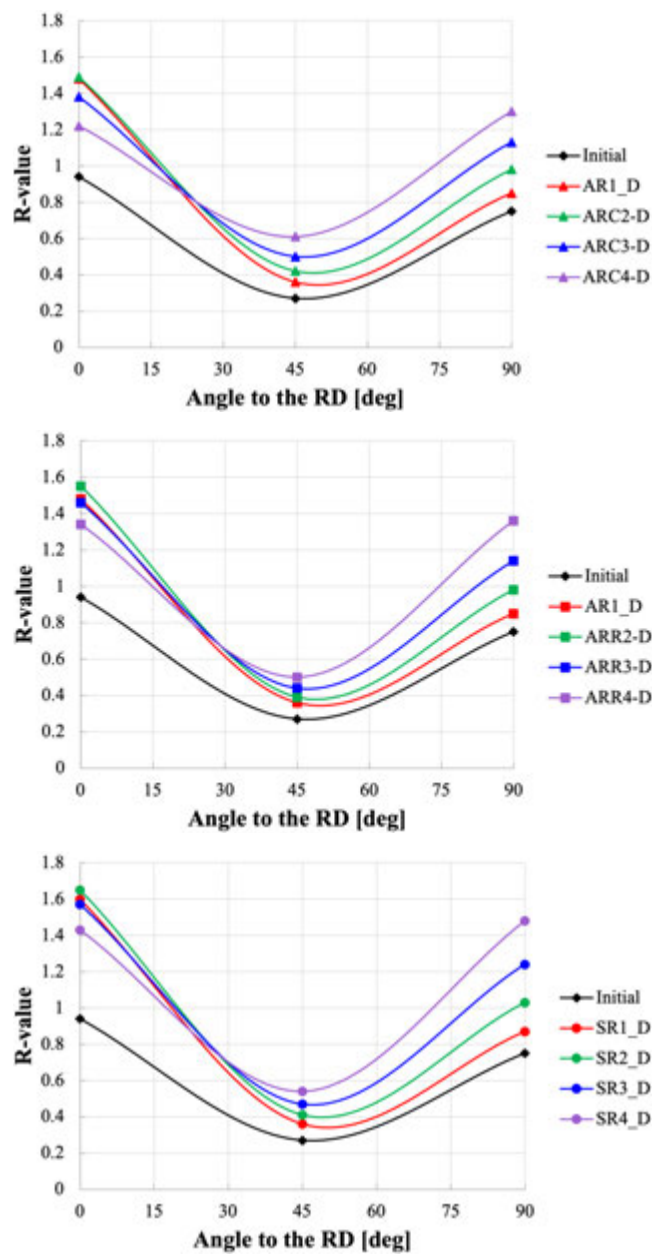
Figure 11   Simulated R-values of four-pass sequences rolling with a 15% thickness reduction per pass of ARC (top), ARR (middle), and SR (bottom) processes using dislocation-based hardening model (D).
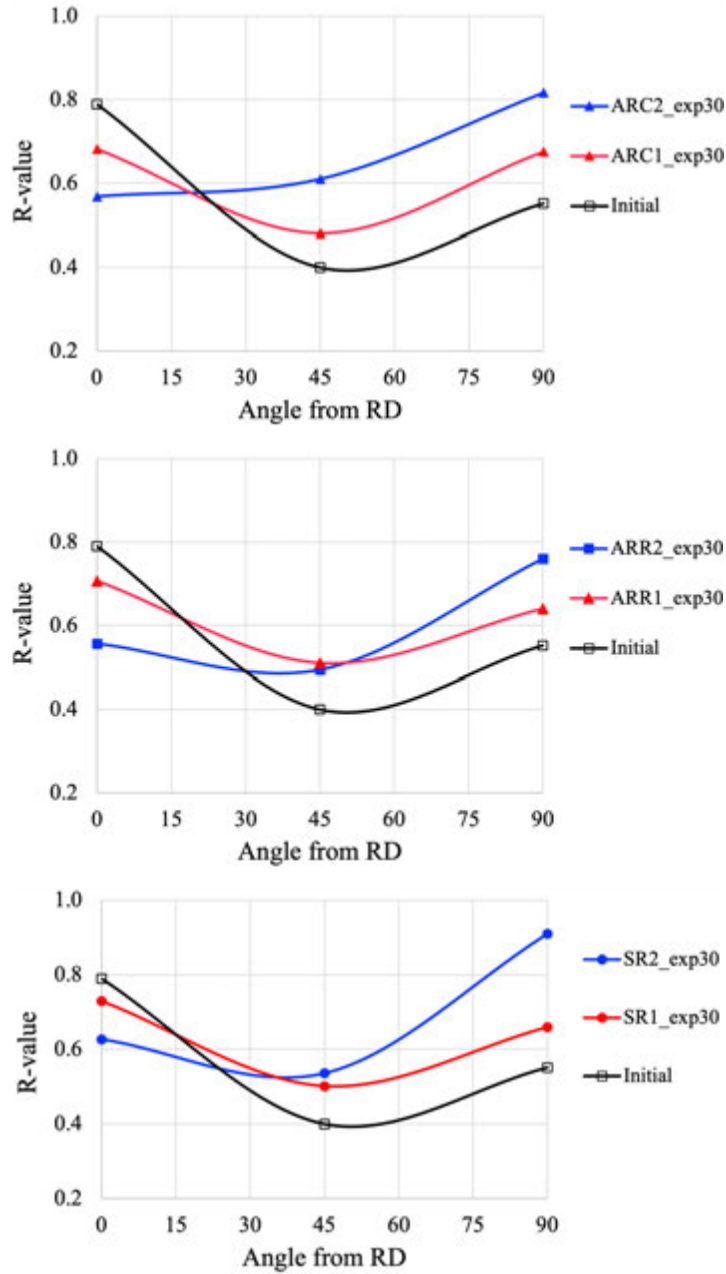
Figure 12 Evolution of Lanckford coefficient with rolling. Experimental data for 30% thickness reduction per pass of ARC (top), ARR (middle), and SR (bottom).
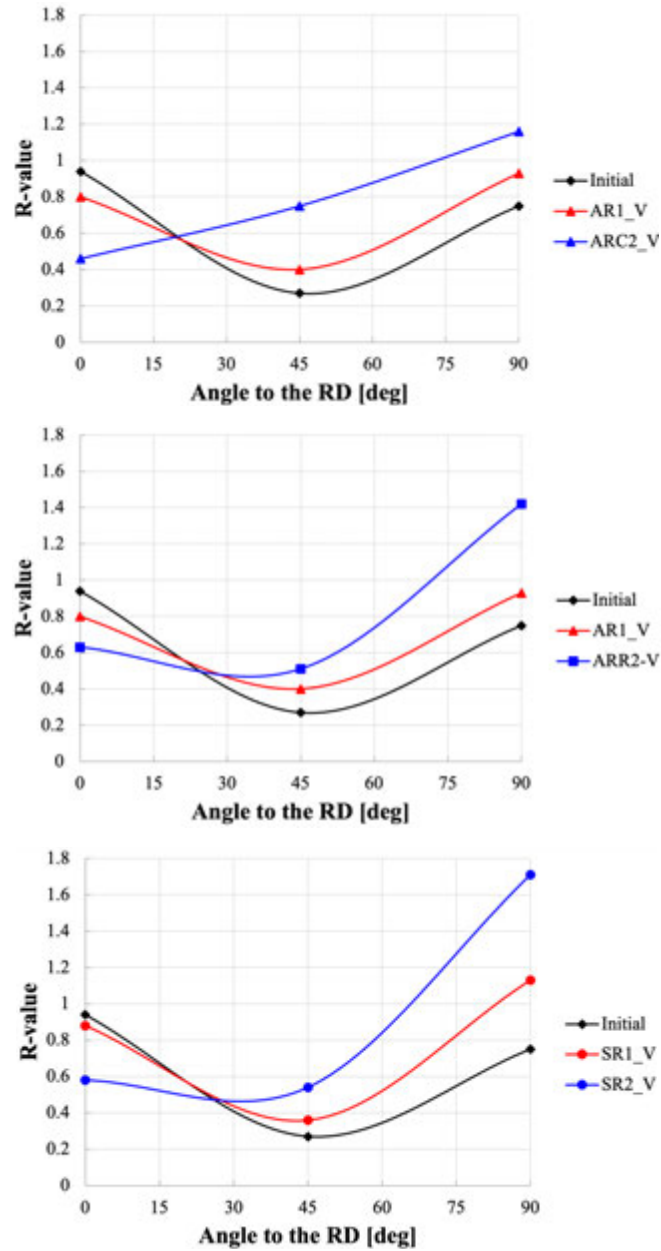
Figure 13   Simulated R-values of four-pass sequences rolling with a 30% thickness reduction per pass of ARC (top), ARR (middle), and SR (bottom) processes using a Voce-type hardening law (V).
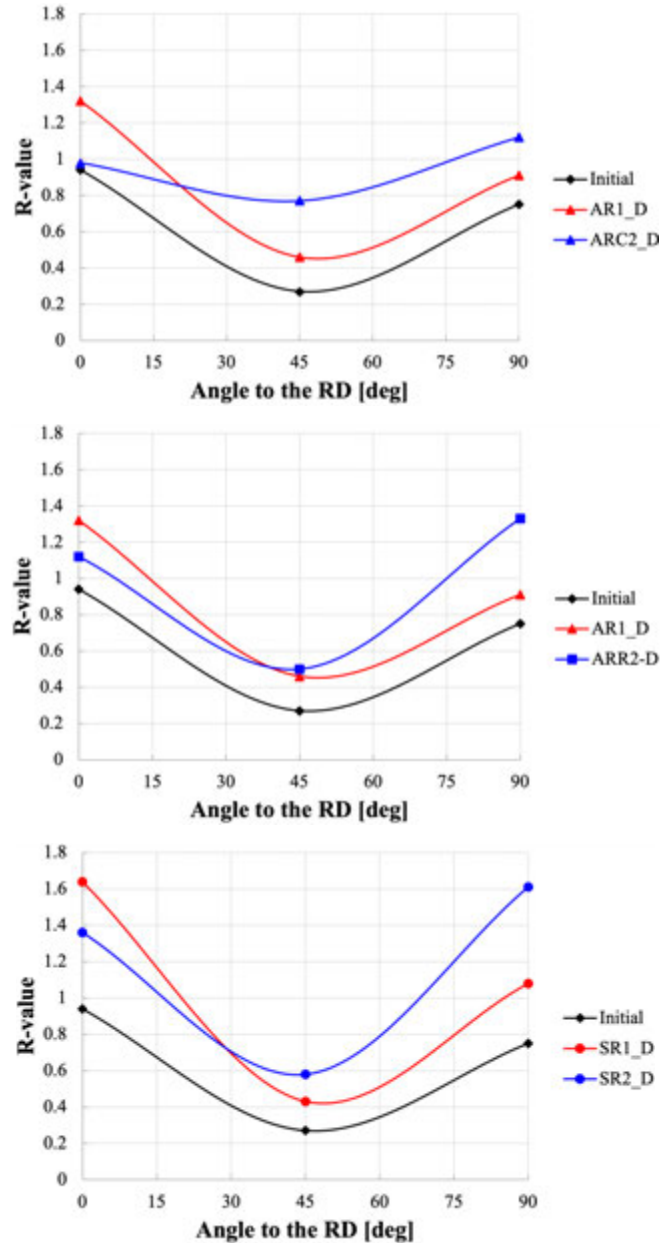
Figure 14 Simulated R-values of four-pass sequences rolling with a 30% thickness reduction per pass of ARC (top), ARR (middle), and SR (bottom) processes using dislocation-based hardening model (D).
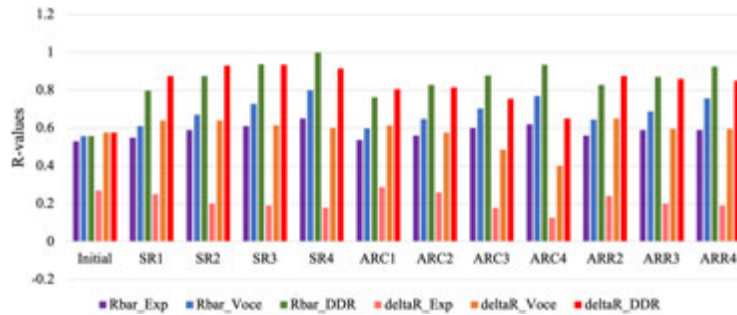
Figure 15 Evolution of normal anisotropy (noted "Rbar" in the graph) and planar anisotropy (noted "deltaR" in the graph) in case of 15% reduction per pass.
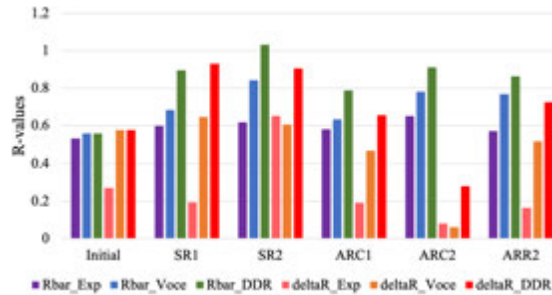
Figure 16 Evolution of normal anisotropy (noted "Rbar" in the graph) and planar anisotropy (noted "deltaR" in the graph) in case of 30% reduction per pass.

values tend to increase and decrease with the number of passes, respectively. This is consistent with the progressive reducion of the cube type texture component intensity with the accumulated passes, measured and predicted by the VPSC model (Figures 17–20). The results also show that the qualitative evolution of the $\overline{R}$ value can be sucesssfully predicted by both hardening laws calculations. However, the Voce type simulations provided values closer (although higher) to the experimental ones and, except for the 30% reduction per pass ARR sequence, correctly predict the progressive decrease of the planar anisotropy with the number of steps. By contrast, in case of DDR, this evolution was obtained only for ARR and SR sequences with, 15% and 30% redution per pass, respectively.

The texture evolution is represented by the ODF sections represented in the Euler angles φ_1, Φ and φ_2. The ideal components of texture represented in the odf sections corresponding to $\varphi_2 = 0$ are Br {011}<211>, Goss {011}<001>, Cube {001}<100>, RCRD1
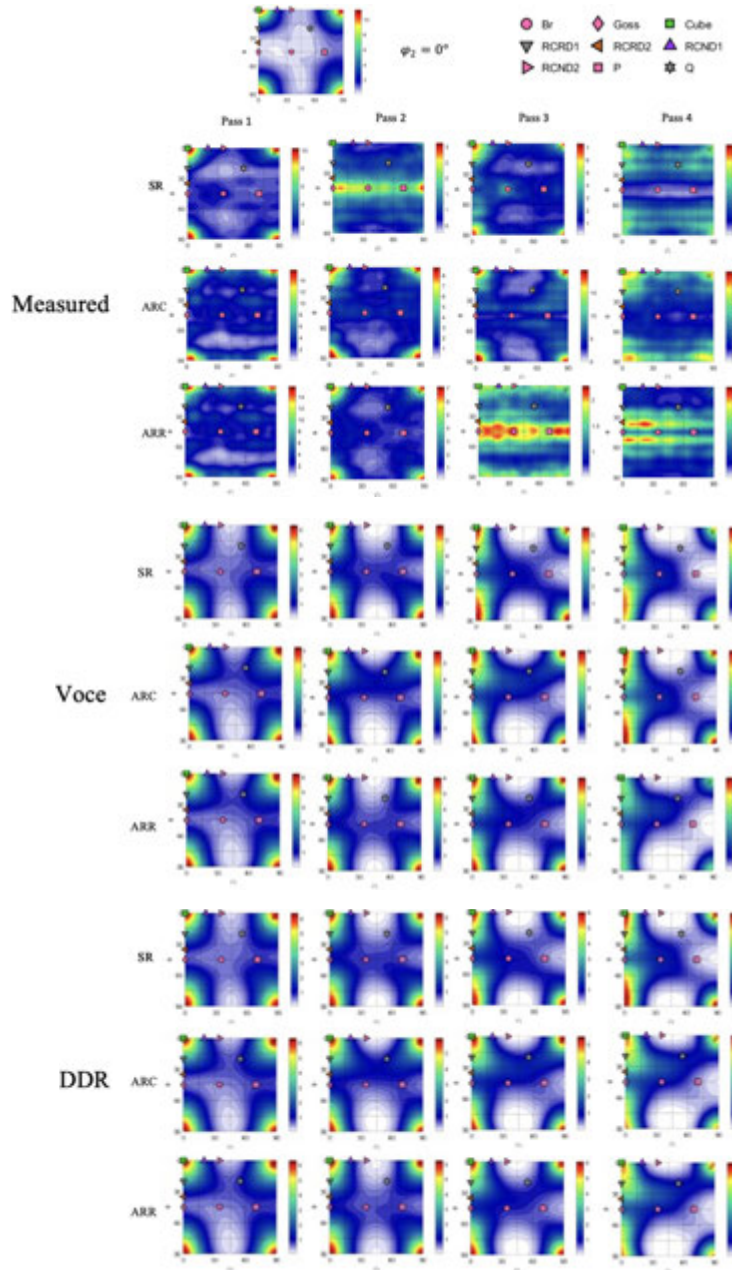
Figure 17 Representation of odf section corresponding to $\varphi_2 = 0°$ after each rolling pass measured (top), simulated with Voce (middle) and DDR (bottom) hardening law.
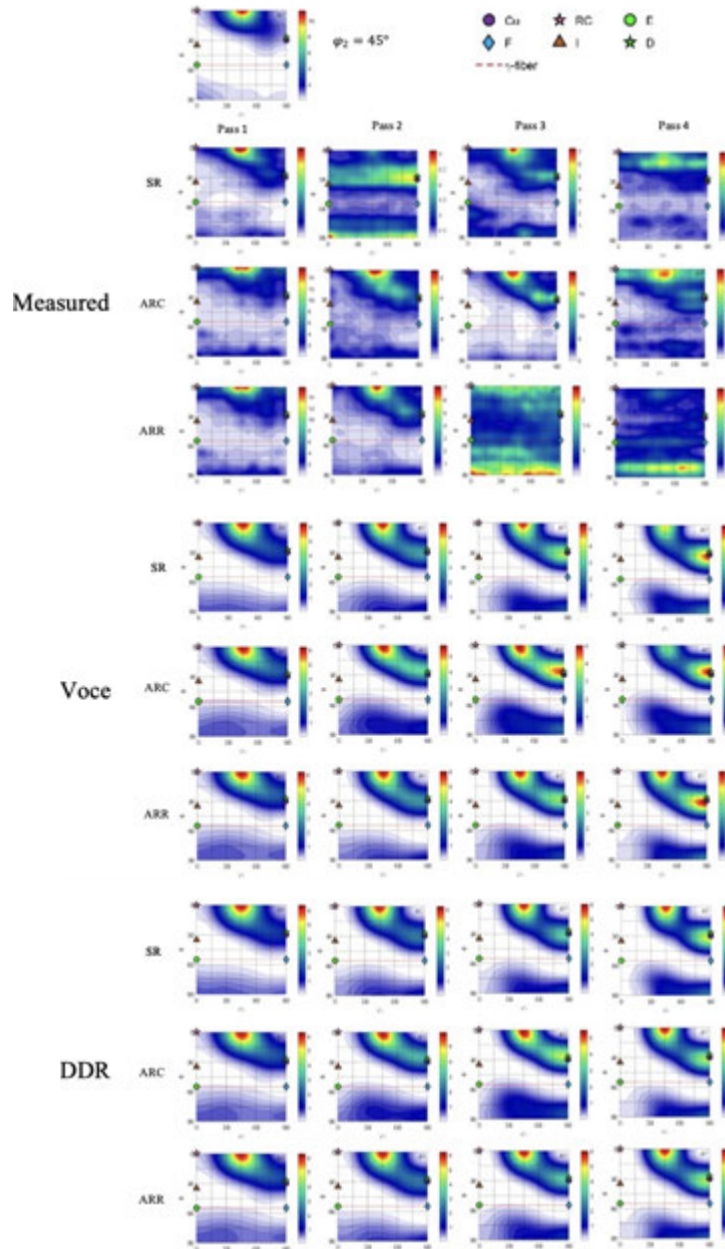
Figure 18   Representation of odf section corresponding to $\varphi_2 = 45°$ after each rolling pass measured (top), simulated with Voce (middle) and DDR (bottom) hardening law.
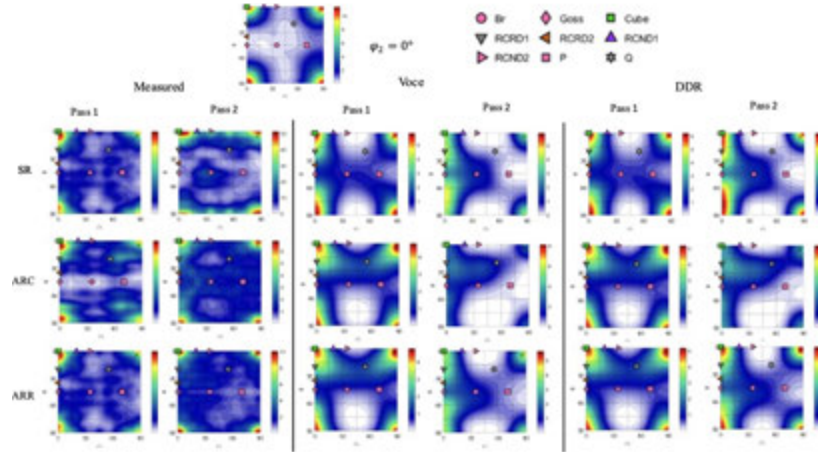
Figure 19 Representation of odf section corresponding to $\varphi_2 = 0°$ after each rolling pass measured (left), simulated with Voce (middle) and DDR (right) hardening law.
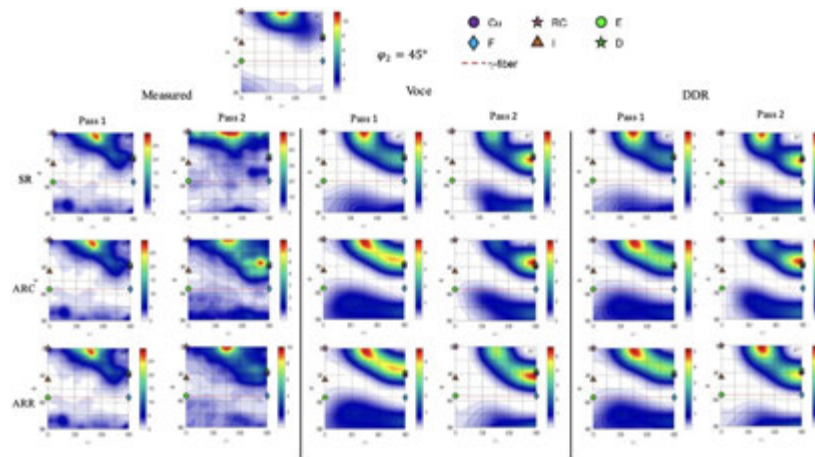
Figure 20 Representation of odf section corresponding to $\varphi_2 = 45°$ after each rolling pass measured (left), simulated with Voce (middle) and DDR (right) hardening law.

{013}<100>, RCRD2 {023}<100>, RCND1 {001}<310>, RCND2 {001}<320>, P {011}<122>, Q {013}<231> and corresponding to $\varphi_2 = 45$ are Cu {112}<111>, RC {001}<110>, E {111}<110>, F {111}<112>, I {112}<110>, D {4 4 11}<11 11 8>.

The cube component is present in every stage of the process, but the intensity decreases with the increase of the number of rolling steps. Other

components such as Goss and rotate cube are formed during the rolling, as can be seen in Figure 17. Since the identification is not very easy, it was evaluated the percentage of these components and it was observed an increase in Goss and rotated Cube components and a decrease in Cube components with the increasing number of passes. This was observed for experimental and numerical results and it can be the reason for the variation of the Lankford coefficient between RD and TD since it agrees with the study of Cazacu et al. [29] in which it is shown that an ideal Goss texture component drastically increases the R-value in the TD direction, and an ideal "rotate cube" texture component decreases the R-value in RD.

4 Conclusion

This work investigated the evolution of R-values during symmetric and asymmetric rolling. A decrease of R-values in RD and an increase in TD is observed for all the rolling routes and it is produced gradually with the increasing number of passes. No effect of the reduction per pass was observed. The Voce-type hardening law incorporated in VPSC is capable to capture better than DDR, the evolution of the R-value with rolling, but returns an overestimated value. The DDR coupled with VPSC, although it succeeded to capture the trend, all the values are way above the ones obtained in experiments. In view of this analysis, it seems that the VPSC model is not the best choice for the analyses of anisotropy evolution during rolling from the quantitative point of view, but it can be used for qualitative analyses.

Acknowledgments

References

[1] R. Hill, 'A theory of the yielding and plastic flow of anisotropic metals', Proc. R. Soc. Lond. A: Math. Phys. Eng. Sci. 193, 281–297, 1948.

[2] F. Barlat, 'Crystallographic texture, anisotropic yield surfaces and forming limits of sheet metals', Mat. Sci. Eng. 91, 55–72, 1987.

[3] F. Barlat, H. Aretz, J.W. Yoon, M.E. Karabin, J.C. Brem, R.E. Dick, 'Linear transformation-based anisotropic yield functions', Int. J. Plast. 21, 1009–1039, 2005.

[4] D. Banabic, F. Barlat, O. Cazacu, T. Kuwabara, 'Anisotropy and formability, in: Advances in Material Forming', Springer, Paris, 143–173, 2007.

[5] O. Cazacu, F. Barlat, 'Generalization of Drucker's yield Criterion to orthotropy', Math. Mech. Sol. 6, 613–630, 2001.

[6] O. Cazacu, F. Barlat, 'Application of the theory of representation to describe yielding of anisotropic aluminum alloys', Int. J. Eng. Sci. 41 (2003) 1367–1385.

[7] O. Cazacu, F. Barlat, 'A criterion for description of anisotropy and yield differential effects in pressure-insensitive metals', Int. J. Plast. 20, 2027–2045, 2004.

[8] G. Sachs, 'Plasticity problems in metals', Trans. Faraday Soc. 24, 84–92, 1928.

[9] G.I. Taylor, 'Analysis of Plastic Strain in a Cubic Crystal', pp. 218–224, Stephen Timoshenko 60th Anniversary Volume, 1938.

[10] C.N. Tomé, R.A. Lebensohn, 'Self-consistent homogenization methods for texture and anisotropy', in: D. Raabe, L.Q. Chen, F. Barlat, F. Roters (Eds.), Continuum Scale Simulation of Engineering Materials, Fundamentals – Microstructures – Process Applications, Wiley, Berlin, 473–499, 2004.

[11] P. Van Houtte, S. Li, O. Engler, 'Taylor-type homogenization methods for texture and anisotropy', in: D. Raabe, L.Q. Chen, F. Barlat, F. Roters (Eds.), Continuum Scale Simulation of Engineering Materials, Fundamentals – Microstructures – Process Applications, Wiley, Berlin, 459–471, 2004.

[12] O. Cazacu, B. Revil-Baudard, N. Chandola, 'A yield criterion for cubic single crystals', Int J. Solids Struct. 10.1016/j.ijsolstr.2017.04.006, 2017.

[13] G. Vincze, F.J.P. Simões, M.C. Butuc, 'Asymmetrical Rolling of Aluminum Alloys and Steels: A Review'. Metals (Basel). 10, 1126, doi: 10.3390/met10091126, 2020.

[14] J. Sidor, A. Miroux, R. Petrov and L. Kestensc, 'Controlling the plastic anisotropy in asymmetrically rolled aluminium sheets'. Philisophical Magazin, 88, 30–32, 2008, 3779–3792, doi: 10.1080/147864308020 64659.

[15] M. Wronski, K. Wierzbanowski, S. Wronski, B. Bacroix, M. Wróbel and A. Uniwersał 'Study of texture, microstructure and mechanical properties of asymmetrically rolled aluminium'. IOP Conference Series: Materials Science and Engineering, 82, Issue 1, 012074, 2015.

[16] M. Wronski, K. Wierzbanowski, S. Wronski, B. Bacroix, P. Lipinski, 'Experimental and finite element analysis of asymmetric rolling of 6061 aluminum alloy using two-scale elasto-plastic constitutive relation'. Arch. Metall. Mater. 2017, 62, 1991–1999, doi: 10.1515/amm-2017 -0297, 2017.

[17] J.-H. Lee, G.-H. Kim, S.K. Nam, I. Kim, D.N. Lee. 'Calculation of plastic strain ratio of AA1050 Al alloy sheet processed by heavy asymmetric rolling–annealing followed by light rolling–annealing'. Comput. Mater. Sci. 100, 45–51. 10.1016/j.commatsci.2014.09.049, 2015.

[18] S. Tamimi, J.P. Correia, A.B. Lopes, S. Ahzi, F. Barlat, J.J. Gracio, 'Asymmetric rolling of thin AA-5182 sheets: Modelling and experiments'. Mater. Sci. Eng. A, 603, 150–159, doi: 10.1016/j.msea.201 4.02.048, 2014.

[19] S.S. Dhinwal, L.S. Toth, 'Unlocking deformation path in asymmetric rolling by texture simulation'. Materials (Basel). 13, 1–7, doi: 10.3390/ ma13010101, 2020.

[20] D. Shore, P. Van Houtte, D. Roose, A. Van Bael, 'Multiscale modelling of asymmetric rolling with an anisotropic constitutive law'. Comptes Rendus – Mec., 346, 724–742, doi: 10.1016/j.crme.2018.06.001, 2018.

[21] F. Bachmann, R. Hielscher, H. Schaeben, 'Texture analysis with MTEX-Free and open source software toolbox'. Solid State Phenom. 2010, 160, 63–68, 2010, doi: 10.4028/WWW.SCIENTIFIC.NET/SSP.160.63.

[22] R.A. Lebensohn, C.N. Tomé, 'A self-consistent anisotropic approach for the simulation of plastic deformation and texture development of

polycrystals-Application to zirconium alloys'. Acta Metall. Mater. 41, 2611–2624, 1993.

[23] R.A. Lebensohn, C.N. Tomé, P. Ponte Castañeda, 'Self-consistent modeling of the mechanical behavior of viscoplastic polycrystals incorporating intragranular field fluctuations'. Philos. Mag. 87, 4287–4322, 2007.

[24] C. Tome, G. R. Canova, U. F. Kocks, N. Christodoulou, and J. J. Jonas, "The relation between macroscopic and microscopic strain hardening in F.C.C. polycrystals," Acta Metall., vol. 32, no. 10, pp. 1637–1653, Oct. 1984, doi: 10.1016/0001-6160(84)90222-0, 1984.

[25] C. N. Tomé and R. A. Lebensohn, "Manual for Code Visco-Plastic Self-Consistent (VPSC), version 7d," Los Alamos National Laboratory, 2018.

[26] E.F. Rauch, J.J. Gracio, F. Barlat, G. Vincze, 'Modelling the plastic behavior of metals under complex loading conditions'. Modell. Sim. Mater. Sci. Eng. 19 (035009), 1–18, 2011.

[27] K. Kitayama, C.N. Tomé, E.F. Rauch, J.J. Gracio, F. Barlat, F., 'A crystallographic dislocation model for describing hardening of polycrystals during strain path changes. Application to low carbon steels', Int. J. Plasticity, 46, 54–69, 2013.

[28] W. Wen, M. Borodachenkova, C.N. Tome, G. Vincze, E.F. Rauch, F. Barlat, J.J. Gracio, 'Mechanical behavior of low carbon steel subjected to strain path changes: Experiments and modeling', Acta Mater., vol. 111, pp. 305–314, doi: 10.1016/J.ACTAMAT.2016.03.075, 2016.

[29] A. Halloumi, C. Desrayaud, B. Bacroix, E. Rauch, and F. Montheillet, 'A simple analytical model of asymmetric rolling', Arch. Metall. Mater., vol. 57, no. 2, pp. 425–435, doi: 10.2478/v10172-012-0042-3, 2012.

[30] O. Cazacu, N. Chandola1, B. Revil-Baudard, 'Analytical expressions for the yield stress and Lankford coefficients of polycrystalline sheets based on a new single crystal model', Int J Mater Form, 11:571–581, doi: 10.1007/s12289-017-1366-3, 2018.

Biographies

Gabriela Vincze received a Ph.D. degree in Mechanical Engineering from Aveiro University. Currently, she works in the same department. Her research focuses on the analysis of materials with emphasis on metallic materials from micro to macro scale and implementation of physical and constitutive models to predict the mechanical behavior of materials for long-term applications. She has been serving as a reviewer for many highly respected journals.

Augusto Lopes received a Ph.D. degree in Materials Science from Aveiro University. Currently, he is an Assistant Professor in the Department of Materials and Ceramics Engineering. His research focuses on the relationship between material structure and the macroscopic behaviour of metals. He has been serving as a reviewer for many highly respected journals.

Marilena C. Butuc received the bachelor's degree in mechanical engineering from University of Timisoara, Romania, in 1993, and the philosophy of doctorate degree in Mechanical Engineering from Faculty of Engineering, Porto University in 2004. She is a Researcher at the Centre for Mechanical Technology and Automation, University of Aveiro, Portugal. Her research areas include sheet metal forming, material modelling and forming limits simulation. She is acting as a reviewer for several prestigious journals.

Jesús Yánez is currently a PhD student and was a research fellow in the project "Enhanced manufacturing of aluminium alloys products for environmentally transportation sector" – POCI-01-0145-FEDER-032362 (PTDC/EME-ESP/32362/2017) which is the main sponsor of the present work. His research interest is related to sheet metal forming of light alloys.

Diogo Lopes was a research fellow in the project "Enhanced manufacturing of aluminium alloys products for environmentally transportation sector" – POCI-01-0145-FEDER-032362 (PTDC/EME-ESP/32362/2017) which is the main sponsor of the present work. His research interest is related to sheet metal forming of light alloys.

Laura Holz is a PhD student in Refining, Petrochemical and Chemical Engineering from Aveiro University. She is an expert in materials' characterization by X-ray diffraction, having a solid background in materials science. Her research interest is related with ceramics for energy-related research. She is the author/co-author of 11 articles in international peer reviewed scientific articles, 4 book chapters, presenting her work in several international conferences.

Ana Graça received a Ph.D. degree in Mechanical Engineering from Aveiro University. She was a researcher in the project "Enhanced manufacturing of aluminium alloys products for environmentally transportation sector" – POCI-01-0145-FEDER-032362 (PTDC/EME-ESP/32362/2017). Her research focuses on computational mechanics with application to metal forming.

Antonio Pereira received a Ph.D. degree in Mechanical Engineering from Aveiro University. Currently, he is an Associate Professor with aggregation in the same department. His research focuses on the mechanics of composite materials, with particular emphasis on delamination fracture mechanics, the plasticity of metals, and welding. He has been serving as a reviewer and editor for many highly respected journals.